ACS NANO

www.acsnano.org

ARTICLE

Molecular Insights into Division of Single Human Cancer Cells in On-Chip Transparent Microtubes

Wang Xi,[*,†,○] Christine K. Schmidt,[*,§,ψ] Samuel Sanchez,[†,▽] David H. Gracias,[‡] Rafael E. Carazo-Salas,[§] Richard Butler,[§] Nicola Lawrence,[§] Stephen P. Jackson,[§,#] and Oliver G. Schmidt[†,∥,⊥]

[†]Institute for Integrative Nanosciences, IFW Dresden, Helmholtzstr. 20, D-01069 Dresden, Germany

[§]The Gurdon Institute and Departments of Biochemistry, Genetics and Pharmacology, University of Cambridge, Tennis Court Road, Cambridge CB2 1QN, United Kingdom

[‡]Department of Chemical and Biomolecular Engineering, Johns Hopkins University, Baltimore, Maryland 21218, United States

[#]The Wellcome Trust Sanger Institute, Hinxton, Cambridge CB10 1SA, United Kingdom

[∥]Material Systems for Nanoelectronics, Chemnitz University of Technology, Reichenhainer Str. 70, D-09107 Chemnitz, Germany

[⊥]Center for Advancing Electronics Dresden, Dresden University of Technology, Georg-Schumann-Str. 11, 01187 Dresden, Germany

Supporting Information

ABSTRACT: ***In vivo*, mammalian cells proliferate within 3D environments consisting of numerous microcavities and channels, which contain a variety of chemical and physical cues. External environments often differ between normal and pathological states, such as the unique spatial constraints that metastasizing cancer cells experience as they circulate the vasculature through arterioles and narrow capillaries, where they can divide and acquire elongated cylindrical shapes. While metastatic tumors cause most cancer deaths, factors impacting early cancer cell proliferation inside the vasculature and those that can promote the formation of secondary tumors remain largely unknown. Prior studies investigating confined mitosis have mainly used 2D cell culture systems. Here, we mimic aspects of metastasizing tumor cells dividing inside blood capillaries by investigating single-cell divisions of living human cancer cells, trapped inside 3D rolled-up, transparent nanomembranes. We assess the molecular effects of tubular confinement on key mitotic features, using optical high- and super-resolution microscopy. Our experiments show that tubular confinement affects the morphology and dynamics of the mitotic spindle, chromosome arrangements, and the organization of the cell cortex. Moreover, we reveal that membrane blebbing and/or associated processes act as a potential genome-safety mechanism, limiting the extent of genomic instability caused by mitosis in confined circumstances, especially in tubular 3D microenvironments. Collectively, our study demonstrates the potential of rolled-up nanomembranes for gaining molecular insights into key cellular events occurring in tubular 3D microenvironments *in vivo*.**

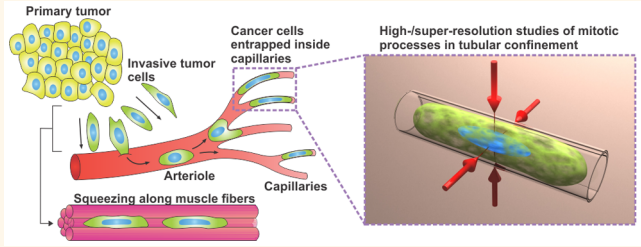

KEYWORDS: *rolled-up nanofilms/membranes, mitosis, chromosome segregation, membrane blebbing, actin cortex, 3D cell culture, metastasis*

Cancer cells, originating from primary lesions can invade adjacent tissues and squeeze along muscle fibers,[1] before entering the vascular system and traveling to distal sites, where some of them can proliferate and form metastases. During this process cancer cells can become trapped inside narrow blood capillaries[2−5] (Figure 1A), where they adapt to the tubular confinement by elongating into cylindrical shapes[6] (Figure 1A and B). Importantly, several *in vivo* studies have shown that circulating tumor cells can divide under such tubular confinements and form early micrometastatic colonies before exiting the vasculature.[2,3] This intravascular proliferation in tubular environments is thought to be a critical step during metastasis, at least in the lung and the liver.[2,3,7−9] Despite the leading role of metastasis in cancer mortality, many steps during this process remain poorly understood. This is due to metastasis being a rare—but often destructive—process that happens in parts of the body not easily accessible to molecular analyses, such as the vascular or

Received: January 20, 2016
Accepted: June 6, 2016
Published: June 6, 2016

DOI: 10.1021/acsnano.6b00461
ACS Nano 2016, 10, 5835−5846

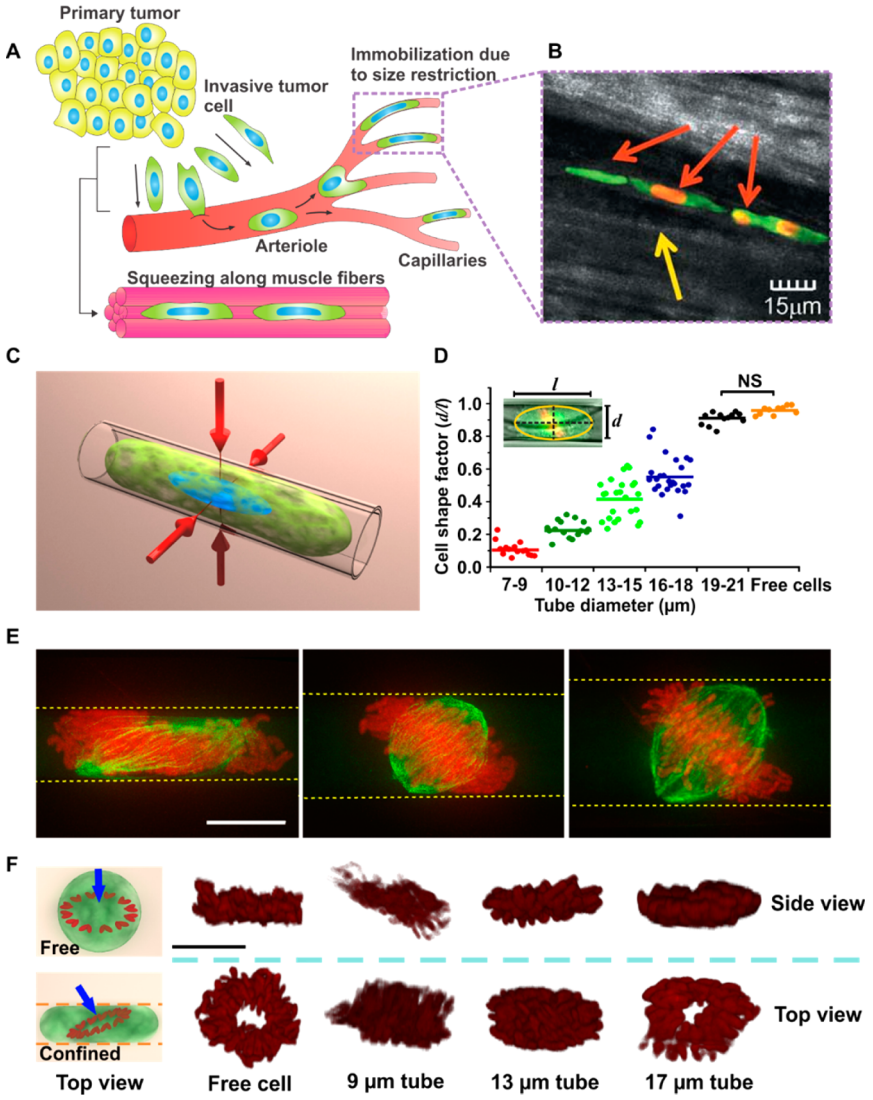

Figure 1. Tubular confinement affects cell shape, chromosome alignment, and spindle morphology in mitotic HeLa cells. (A) Schematic of metastasizing tumor cells originating from the primary tumor and circulating the blood system. The large tumor cells get trapped, for instance, through size restriction, in narrow capillaries, where they acquire elongated cylindrical shapes. (B) Dual-labeled cancer cells (red: nuclei; green: cytoplasm) trapped inside a blood capillary in a living mouse. The cells were imaged 1 h after injecting them in the epigastric cranialis vein in an abdominal skin flap. The cells and nuclei are deformed by elongation to fit the small (~8 μm) inner diameter of the capillary. Yellow arrow indicates the outer wall of the blood vessel. Red arrows point out entrapped and elongated human HT-1080 dual-color cells. The right red arrow indicates a cell that has likely undergone mitosis, as judged by its binucleate appearance. Image taken from Suetsugu et al., 2013.[6] Reprinted with permission from ref 6. Copyright 2013 The International Institute of Anticancer Research. (C) 3D schematic of tubular confinement, indicating 2D constraints (red arrows) on 3D cultured mammalian cells. (D) Cell shape factor plotted against microtube sizes (n = 15, 16, 24, 25, 12, and 10 cells from left to right). The inset shows an ellipsoidal fit in orange and black dashed lines for the major (l) and minor (d) ellipsoid axes. NS, not significant; all other cell shape factors are significantly altered compared to free cells (p-value < 0.05; Student's t-test). (E) 3D projected fluorescent microscopy images (histone H2B-mCherry, red; GFP-tubulin, green) of prometa-/metaphase HeLa cells inside differently sized rolled-up nanomembranes (regions between the parallel, dashed lines). (F) Side (upper row) and top (lower row) 3D reconstructed images of chromosome rosettes inside different microtube sizes. The 3D schematics on the left indicate the top view angles (blue arrows) for free (top) and confined (bottom) chromosome rosettes depicted in the lower row on the right. Scale bars, 10 μm.

ductal system. Gaining molecular insights into how 3D, and in particular tubular, constraints affect the division of human cancer cells might therefore lead to a better understanding of the events and factors that promote metastasis, which in the future could help improve antimetastatic cancer treatments.

Cell division, the partitioning of the nucleus (mitosis) followed by the division of the cytoplasm (cytokinesis), involves striking 3D changes in the cell's geometry and cytoskeleton. For instance, most dividing eukaryotic cells restructure their interphase actin structures,[10] resulting in the recruitment of actin filaments to the cell cortex,[11] thereby imparting a heightened stiffness to mitotic cells.[12,13] This increased rigidity is usually accompanied by conspicuous changes in mitotic cell shape, whereby the cells abandon their flattened and spread-out interphase morphologies on planar substrates to take up rounded-up sphere-like shapes.[14,15] The cell cortex is then further remodeled to generate a contractile

DOI: 10.1021/acsnano.6b00461
ACS Nano 2016, 10, 5835−5846

actomyosin ring that is tightly coupled to the plasma membrane[11] and enables cytokinesis.[16]

Mitotic rearrangements of the cortex are accompanied by, and tightly linked to, the remodeling of the interphase microtubule network into a bipolar spindle, which itself possesses an intricate 3D architecture. Dedicated motor-protein activities functioning along microtubules help to provide the vectorial forces required to push/pull the duplicated centrosomes apart, allowing the centrosomes to migrate along various 3D trajectories to opposite cell poles. This process occurs in a tightly controlled temporal manner and generates a mature prometa-/metaphase spindle with extremely well-defined geometric dimensions.[17−19] A ring-like arrangement of chromosomes then forms at the nascent spindle, facilitating bipolar attachment of microtubules to the chromosomes' kinetochores and, thus, enabling faithful chromosome segregation and maintaining genomic stability.[17] Notably, genomic instability can lead to cancer as well as other diseases,[20,21] highlighting the importance of genome-protective mechanisms for human health.

Mitotic progression is highly sensitive to external physical influences, such as spatial stimuli and geometric constraints.[22−24] Indeed, by remodeling the actin cortex lying at the interface between an animal cell and its environment, mitotic cells can translate geometric aspects of their microenvironment into spatial information that determines the fate of their daughter cells. For instance, the pattern of cell adhesion can dictate the orientation of the spindle and thus, the positions of the two arising daughter cells.[22,24] Moreover, preventing mitotic cell rounding by planar compression in one dimension from the top/bottom can cause mitotic delays, multipolar spindles, and defects in chromosome segregation.[14,25] In addition, changes in spindle architecture caused by external forces[26] can impair the stability of the bipolar spindle and the positioning of the cell division plane.[14]

Collectively, the above findings illustrate tight connections between the cortical cytoskeleton and spindle microtubules and the highly mechanosensitive nature of cell division. However, prior studies were mainly performed on cells growing on flat surfaces that lack the geometric attributes of the highly curved substrates and tubular confinements cells experience inside the body, such as kidney tubules, mammary ducts, gut villi, vessels, muscle fibers, and bone tissue. Despite the *in vivo* relevance of these microenvironments, only few *in vitro* models have been developed to mimic the geometry of such structures, for instance, the ducts and acini of mammary glands.[27] Importantly, recent evidence has emerged indicating that cells under tubular confinement elicit distinct mitotic responses to external spatial stimuli that are different compared to those of spatially confined cells growing on planar substrates.[28] Investigating these responses at a molecular level is therefore crucial to understand better how the physical parameters of different 3D surroundings, such as the tubular confinement of cancer cells inside blood capillaries (Figure 1B), might dictate mitotic cell behavior and function.

To address this challenge, we have developed and used rolled-up SiO/SiO_2 nanofilms to encapsulate live, individual human cancer cells (HeLa cells) inside transparent microtubes[28−30] (Figure 1C). This tubular nanomembrane system offers a way of mimicking aspects of the *in vivo* 3D microenvironments certain cancer cells encounter during metastasis. The behavior of the entrapped cells can then be analyzed conveniently with high- and super-resolution microscopy. Moreover, due to the on-chip nature of the platform, numerous cells can be imaged in a single experiment. Other systems, such as microfluidic devices, either have complex macro-to-micro interfaces, introduce contamination *via* oil molecules, have rectangular rather than circular channels, or cannot be implemented in an easily visualizable chip-based format.[31−33]

In this study, we show that tubular confinement has a profound impact on a wide range of mitotic features, and we provide an in-depth characterization of these features at a molecular level by using confocal and super-resolution 3D structured illumination microscopy (3D SIM). Thus, we observed deformation of chromosome rosettes into densely packed and disordered shapes and show that tubular confinement influences the kinetics of spindle formation. In addition, consistent with the link between the mitotic spindle and the cell cortex, we discover a striking bipolar redistribution of cortex proteins that occurs specifically in mitotic cells dividing inside nanomembrane tubes. This redistribution coincides with conspicuous membrane blebbing that occurs at the actin- and cortactin-enriched cell tips throughout mitosis. Finally, we establish that membrane blebbing and/or associated processes can act as a potential genome-safety mechanism that becomes functionally important under certain spatial confinements. Based on our findings, we discuss the potential of our platform for uncovering cellular pathways relevant for cells dividing in certain 3D microenvironments. These advances might help provide a better understanding of the molecular events happening, for instance, during early intravascular proliferation of circulating tumor cells.

RESULTS AND DISCUSSION

Tubular Confinement Impacts on Mitotic Cell Rounding, Spindle Morphology, and Chromosome Arrangements. To gain insights into how spatial confinement influences key mitotic features of cells dividing in 3D contexts, we fabricated arrays of on-chip microtubes, inside which individual proliferating human cells, such as HeLa cells, can be entrapped and cultured[28] (Figure 1C). Briefly, SiO/SiO_2 nanobilayers of 25−100 nm thickness were deposited on a transparent substrate patterned with 100 × 100 μm square-shaped sacrificial layers. After selective etching away of the sacrificial layers, the SiO/SiO_2 nanobilayers were self-folded into microtubes in on-chip format with a density of ∼500 microtubes per 1 cm^2 chip area.[34−36] The diameters of microtubes are highly defined and tunable.[30] We used 7−21 μm microtubes in our initial experiments, because 7 μm represents about one-third of the diameter of rounded-up human HeLa cells (∼20 μm) and because we found that nanomembrane tubes of this size are the smallest tubes that HeLa cells can be entrapped in (not shown). By contrast, tubes with diameters above 21 μm do not impose any spatial confinement on mitotic HeLa cells, as they are larger than the rounded-up diameter of HeLa cells during mitosis. The surfaces of the microtubes were functionalized with fibronectin to mimic aspects of the chemical microenvironment of mammalian cells *in vivo*. We then co-cultured HeLa cells with the nanomembrane arrays overnight, allowing the cells to spontaneously migrate into the tubular nanomembranes.[28] Finally, we analyzed cells entrapped inside the tubes with high-resolution fluorescence microscopy (confocal microscopy) and/or super-resolution 3D SIM. As described below, these techniques

DOI: 10.1021/acsnano.6b00461
ACS Nano 2016, 10, 5835−5846

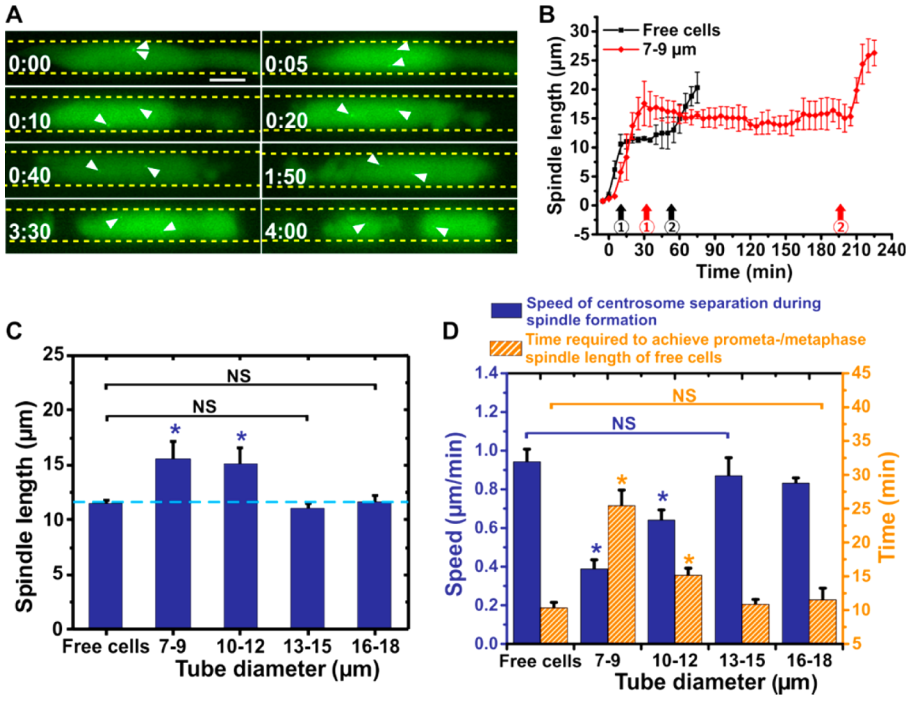

Figure 2. Tubular confinement perturbs the kinetics of centrosome separation during spindle formation and leads to abnormally elongated prometa-/metaphase spindles. (A) Time-lapse *z*-stack projections of a HeLa cell dividing inside a 9 μm microtube and expressing centrin1-GFP (green; white arrowheads), a centrosome marker, to visualize the 3D spindle pole kinetics in the cell. Scale bar, 10 μm. Times are in hour:min format. (B) Quantification of (A) showing the temporal evolution of spindle length (mean 3D distances between centrosomes ± SD; time '0' defined as the beginning of cell rounding) in the indicated situations. The ①s with arrows indicate the times at which full separation of the centrosomes is achieved in prometa-/metaphase, *i.e.*, when a mature prometa-/metaphase spindle has formed (black ①: 10.3 ± 0.8 min for free cells and red ①: 32.3 ± 2.1 min for cells in 7−9 μm microtubes). The onset of anaphase spindle elongation is marked by a black and red ② for free cells and cells confined in 7−9 μm microtubes, respectively. In each case, the experiment was repeated at least five times. (C) Quantification of prometa-/metaphase spindle lengths ± SD in the indicated spatial environments (n = 7, 6, 6, 5, and 5 cells from left to right). Blue dotted line indicates the average spindle length corresponding to free cells. (D) Bar graph illustrating average elongation speeds of nascent spindles in indicated spatial environments (blue columns; n = 7, 6, 6, 5, and 5 cells from left to right) and the average time required to form an 11.5 μm long spindle, the average length of prometa-/metaphase spindles in free cells (orange columns; n = 7, 6, 6, 5, and 5 cells from left to right; mean ± SD; see Supplementary Figure 3C for more details). NS, not significant, *significantly altered changes compared to free cells (p-value < 0.05; Student's *t*-test).

allowed us to gain insights into key processes occurring during single-cell division under tubular confinement.

The rolled-up nanomembrane configuration enables tubular 2D-confinement of 3D cultured mitotic human cells (Figure 1C). As such, the nanomembrane platform is fundamentally different from previous 1D-confined (from top and bottom) experimental set-ups based on cells cultured on 2D/planar surfaces[14,25] (Supplementary Figure 1). We observed that confinement inside tubular nanomembranes prevented cells from rounding up during mitosis. Instead, cells adopted elongated cylindrical shapes, as illustrated by the strong correlation between the cell shape factor (ratio between the minor and major axes of an ellipse fitted to the cell) and the microtube diameter (Figure 1D). We therefore focused our subsequent analyses on microtube diameters ranging from 7 to 18 μm, the largest microtubes that induced significant cell shape changes (Figure 1D). Significantly, this diameter range is comparable to the widths of *in vivo* blood arterioles/capillaries present in humans and other mammals.[5,6,37] While blood capillaries readily allow passage of endogenous cells of the vascular system, such as red blood cells (~7 μm in diameter), metastasizing cancer cells that are much larger in diameter (~20 μm) can get stuck due to size restriction.[4,5] Importantly, cancer cells trapped inside the vascular system adapt to the widths of blood capillaries *in vivo*,[37] comparable to HeLa cells encapsulated by narrow rolled-up nanomembranes. Thus, the extent of deformation of cancer cells inside blood capillaries in living organisms matches well with the changes in cell shape we observed inside rolled-up nanomembranes: cell shape factors reached ~0.08 in the very narrowest vascular capillaries inside living mice,[37] comparable to the ~0.10 cell shape values we determined for HeLa cells inside 7−9 μm rolled-up nanomembranes (Figure 1D). Collectively, these findings illustrate that the experimental conditions in our system are within the range of tubular constrictions certain cells encounter *in vivo*.

To probe how tubular confinement affects the mitotic machinery in 3D cultured cells, we investigated how the obstruction of cell rounding influences spindle morphology and chromosome alignment in mitotic prometaphase and metaphase (named prometa-/metaphase henceforth). Both spindle and chromosome alignments are geometrically demanding features that are important for successful mitotic progression.[11,38−40] For our experiments, we used HeLa cells stably co-expressing the core histone H2B tagged with the fluorescent marker mCherry (H2B-mCherry) and α-tubulin fused to green fluorescent protein (GFP-tubulin). This allowed us to simultaneously follow chromosome and spindle dynamics by fluorescence microscopy together with morphological cell shape changes (Figure 1E). The acquired images revealed that tubular confinement often led to misaligned chromosome

DOI: 10.1021/acsnano.6b00461
ACS Nano 2016, 10, 5835−5846

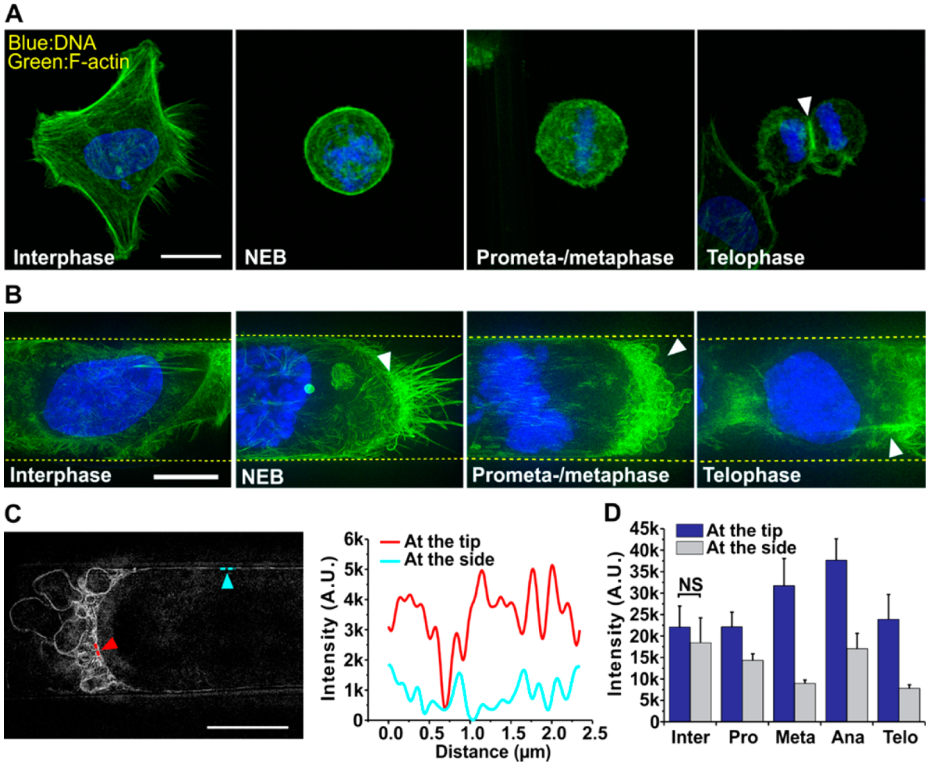

Figure 3. Tubular confinement induces bipolar distribution of cortical actin in mitotic HeLa cells. (A) Confocal images of phalloidin-stained free HeLa cells showing the distribution of actin filaments (F-actin) in indicated cell cycle phases (blue: DAPI staining to visualize DNA). Enrichment of F-actin at the cytokinetic furrow is highlighted by a white arrowhead. (B) Super-resolution 3D SIM projection images of confined human HeLa cells. Stainings and cell cycle stages as in (A). White arrowheads point to enrichment of F-actin at cell tips. (C) Left: Super-resolution fluorescent image showing bipolar distribution of actin filaments at the cell tip of a confined metaphase HeLa cell in a 3D SIM single *z*-plane. Right: Fluorescence intensity profiles along the blue (cell side) and red (cell tip) dotted lines, as indicated in the left image by arrowheads. Note the enrichment of F-actin at the cell tip facing the opening of the rolled-up nanomembrane. (D) Histogram of mean fluorescence intensities (±SD) of F-actin at 30 randomly chosen locations at the sides and tips of HeLa cells (fluorescence intensity sums along 0.5 μm lines at different locations as shown in (C)) in indicated cell cycle phases of HeLa cells confined within 13−15 μm microtubes. NS, not significant; comparisons of F-actin intensities between the cell tip and the side for all mitotic cell cycle phases are significantly different (p-value < 0.05; Student's *t*-test). Scale bars, 10 μm. A.U., arbitrary units.

plates and variations in the angles between metaphase plates and spindle axes (Figure 1E). 3D chromosome reconstructions highlighted a strong compression of prometaphase chromosome arrangements inside microtubes below 13 μm in diameter (Figure 1F and Supplementary Movies 1−4). During early prometaphase, unconfined HeLa cells dividing on planar surfaces outside of the microtubes (named "free cells" henceforth) displayed typical chromosome rosettes, ring-shaped chromosome formations of ∼10 μm in diameter (extracted from our live- and fixed-cell observations). The rosettes consistently formed at the surface of nascent spindles, with the arms pointing outward and the centromeres inward toward the spindle axis, in accord with previous reports[17] (Figure 1F; Supplementary Figures 2A and B, left and Supplementary Movie 1). These rosettes are believed to be crucial for timely establishment of bipolar kinetochore attachments to opposite spindle poles, a process that relies on a functional prometaphase spindle and is important for faithful sister chromatid segregation.[17,41] Chromosomes captured from this ring by the microtubules are concentrated to form a metaphase plate at an angle perpendicular to the long axis of the spindle.[17] Only when all kinetochores are properly bioriented and the spindle assembly checkpoint (SAC) is satisfied, do cells enter anaphase, triggering a loss of sister chromatid cohesion and the movement of sister chromatids to opposite cell poles.[42] By contrast, 3D reconstructions of cells confined inside microtubes of <14 μm diameters did not contain chromosome rosettes. Instead, their chromosomes exhibited dense packaging into tilted plates lacking a central cavity (Figure 1F and Supplementary Movies 2−4). These effects were pronounced most strongly in nanomembrane tubes narrower than 10 μm, the mean diameter of chromosome rosettes in free HeLa cells. In those narrow microtubes, the prometaphase chromosome arrangements appeared twisted and strongly elongated into "cloud-like" structures (Figure 1F, Supplementary Figure 2B, right and Supplementary Movie 2).

Tubular Confinement Impacts on the Dynamics of Centrosome Separation. Chromosome rosettes are important for the timely formation of bipolar prometa-/metaphase spindles.[17] Thus, we wondered whether tubular confinement impacts on the kinetics of spindle formation. To address this question, we took advantage of a Fiji plugin (http://fiji.sc; Fiji is an open source software that is a bundled version of Image J) to automatically monitor the 3D motion of centrosomes during mitosis, using GFP-tagged centrin1 as a marker (centrin1-GFP; Figure 2A, Supplementary Figures 3A and B and Supplementary Movies 5 and 6). The evolution of spindle length—the distance between the two centrosomes—revealed three distinct phases during mitosis (I−III; Supplementary Figure 3C). This allowed us to determine the timing of the transition from an

DOI: 10.1021/acsnano.6b00461
ACS Nano 2016, 10, 5835−5846

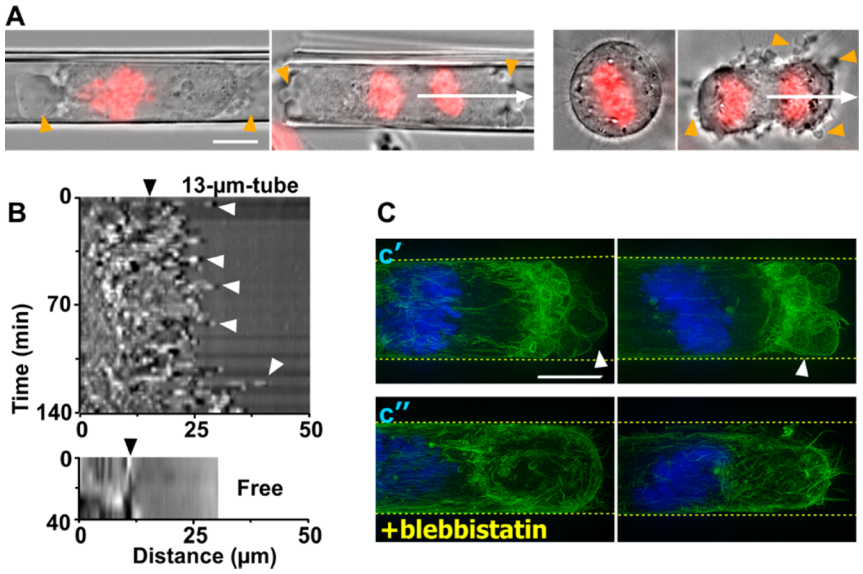

Figure 4. Tubular confinement induces marked membrane blebbing at the tips of mitotic HeLa cells. (A) Spatially confined cells show conspicuous blebbing from prometaphase onward (left two images), whereas unconfined HeLa cells start blebbing only during cytokinesis (right two images). Membrane blebs are highlighted by orange arrowheads. H2B-mCherry is shown in red. For white arrows see description in (B). (B) Kymographs of 10 pixels in width along longitudinal cell axes of HeLa anaphase cells (white arrows in A) were created from phase-contrast time-lapse movies: every 3 min for 140 min for a representative 13 μm microtube confined cell (top); every 3 min for 40 min for a representative free cell (bottom), starting from NEB and cell rounding to the end of telophase. Distance '0' indicates the center of the rounded-up cells just after NEB. Black arrowheads indicate initial cell membrane position at NEB, and white arrowheads indicate protrusions of membrane blebs. (C) Super-resolution 3D SIM images of confined HeLa cells (DAPI, DNA, blue; phalloidin, F-actin, green) with conspicuous blebs at cell tips in prometa-/metaphase (two representative cells) in the absence (c′) or presence (c″) of 25 μM blebbistatin. Scale bars, 10 μm.

elongating nascent spindle to a prometa-/metaphase spindle, which is fairly constant in length (Figure 2B and Supplementary Figure 3C). The ①s with arrows indicate the times at which full separation of the centrosomes is achieved in prometa-/metaphase *i.e.*, when a mature prometa-/metaphase spindle has formed (Figure 2B and Supplementary Figure 3C). Moreover, the data indicated the timing for initiation of the final elongation phase of the spindle during anaphase (Figure 2B and Supplementary Figure 3C, time points indicated with ②). We found that tubular confinement prolonged the formation of prometa-/metaphase spindles from 10.3 ± 0.8 min in free cells (black ①, Figure 2B) around 3-fold to 32.3 ± 2.1 min in cells dividing inside narrow microtubes below 10 μm (red ①, Figure 2B). We detected an intermediate, around 2-fold, delay to 20.0 ± 5.0 min in cells dividing inside microtubes between 10 and 12 μm (Supplementary Figures 3C and D, time points indicated with ①).

The delays in intermediate and narrow sized tubes were significant compared to free cells (p-value < 0.0009, Student's *t* test) and could be explained by either or both of two phenomena: first, elongated prometa-/metaphase spindles; and second, slower elongation speeds of nascent spindles. To address the first possibility, we measured the lengths of prometa-/metaphase spindles in cells exposed or not exposed to tubular confinement. Ensuing analyses revealed that, in <10 μm and 10−12 μm microtubes, prometa-/metaphase spindles were ∼4 μm longer than those of free cells (Figures 2B and C, and Supplementary Figures 3B−D). To address the second possibility, we compared the elongation speeds of nascent spindles in cells dividing without or with tubular confinement. Experiments revealed that the mean elongation speed of nascent spindles was significantly reduced from 0.94 ± 0.06 μm/min in free cells to 0.39 ± 0.05 μm/min in 7−9 μm microtubes and 0.64 ± 0.05 μm/min in 10−12 μm microtubes (Figure 2D, blue columns; see Supplementary Figures 3C and D for more information). Under the tightest confinement conditions, the reduction in elongation speed led to a 15 min delay in forming spindles of lengths similar to those of free cells (Figure 2D, orange columns; see Supplementary Figures 3C and D for more information). This time difference is comparable to the delay in spindle formation predicted by computational simulations of *in silico* perturbations of chromosome rings.[17] We conclude that the observed spindle formation delays inside rolled-up nanomembranes are likely due to a combined effect of elongated prometa-/metaphase-spindle lengths and decreased elongation speeds during spindle formation. Moreover, these elongated prometa-/metaphase spindles inside narrow microtubes plateaued for extensive time periods before further elongating in anaphase (Figure 2B and Supplementary Figures 3C and D). These findings thus demonstrate that increased durations of spindle formation as well as strongly prolonged prometa-/metaphases contribute to the extensive overall mitotic delays occurring inside rolled-up nanomembranes.[28]

Bipolarization of the Mitotic Actin Cortex Inside Rolled-Up Nanomembranes. Mitosis is a geometrically demanding process. As such, it is spatially controlled to ensure that two equivalent daughter cells are produced with high fidelity and in various situations placed into spatially favorable positions. Cells can sense physical cues in their environment to adjust their cytoskeleton.[43] Thus, we tested whether and/or how the cytoskeletal cortex of mitotic cells was affected by tubular confinement. To do so, we stained different mitotic stages of free and confined HeLa cells for actin, a major cytoskeletal protein. Based on confocal and 3D SIM approaches, we performed high- and super-resolution imaging

DOI: 10.1021/acsnano.6b00461
ACS Nano 2016, 10, 5835−5846

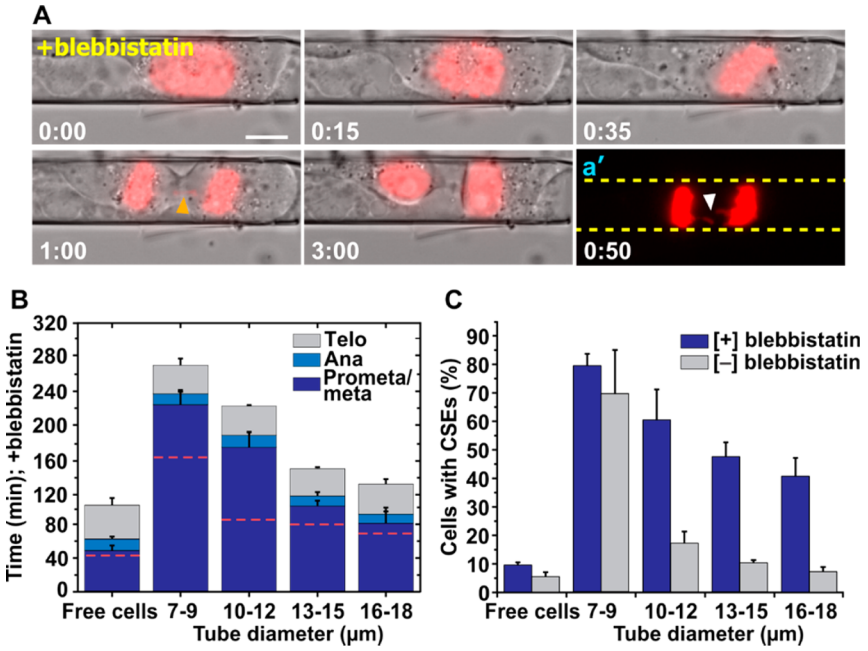

Figure 5. Membrane blebbing and/or associated processes limit the extent of chromosome segregation errors inside rolled-up nanomembranes. (A) Typical time-lapse images (phase-contrast and fluorescently tagged H2B-mCherry, red) of a mitotic HeLa cell, displaying CSEs (orange arrowhead) in the presence of blebbistatin in a 16 μm microtube. Lagging chromosomes (white arrowhead) in anaphase in the same cell are highlighted more clearly in a′ (H2B-mCherry; red). Scale bar, 10 μm. Times are shown in hour:min format. (B) Quantification of mean durations of mitotic phases (±SD) in blebbistatin-treated cells (n = 46, 15, 7, 20, 18 cells from left to right). Red dotted horizontal lines indicate corresponding average prometa-/metaphase durations in the absence of blebbistatin (taken from ref 28). (C) Histogram of mean percentages (±SD) of blebbistatin-treated anaphases with CSEs (n = 96, 26, 18, 38, 27 anaphase cells from left to right). CSEs in HeLa anaphase cells in the absence of blebbistatin (taken from ref 28) are shown as a reference (gray bars).

of actin filaments (F-actin). In free HeLa cells, the overall distribution of F-actin at the cortex (green, labeled by phalloidin) remained uniform in different mitotic stages until the formation of the contractile ring in telophase (see Figure 3A for representative images). By contrast, in confined cells we detected a remarkable enrichment of cortical F-actin at the cell tips, facing the open ends of the microtubes. This bipolar accumulation was reproducibly observed from nuclear envelope breakdown (NEB) onward until telophase, and was specific to mitosis, since no such enrichment was present in confined interphase cells (Figure 3B, left image). Moreover, the bipolar distribution of actin did not affect formation of the contractile ring in telophase. A similar staining pattern was observed for cortactin, a monomeric protein involved in actin polymerization. Thus, it appears that, under tubular confinement, related, but distinct, cytoskeletal proteins are rearranged in a similar fashion to one another (Supplementary Movie 7). To quantify this redistribution, we measured the fluorescent intensities of phalloidin in single 3D SIM cross sections of mitotic HeLa cells. This revealed a more than 2-fold higher F-actin accumulation at the cell tips (Figure 3C, red arrowhead) compared to the sides underlying the microtube walls (Figure 3C, light-blue arrowhead). The fluorescence intensities along 0.5 μm xy cortex sections at different locations and their evolution through mitosis are presented in Figure 3D. We observed this phenomenon in both transformed HeLa cells and nontransformed human retinal pigment epithelial (RPE1) cells (Supplementary Figure 4), suggesting that the bipolar accumulation of certain cytoskeletal proteins under tubular confinement might be a phenomenon conserved among various cell types. In line with spindle orientation being tightly linked to the distribution of the cortex (see Introduction), we noticed that misaligned spindles in confined cells reorientated themselves toward the enriched cortex, facing the open ends of the rolled-up nanomembranes (Supplementary Figure 5).

Conspicuous Membrane Blebbing of Mitotic Cells Inside Rolled-Up Nanomembranes. The bipolar enrichment of actin and cortactin inside rolled-up nanomembranes was accompanied by conspicuous membrane blebbing (Figure 3B and C, left), with the cell membrane at the tips of the confined dividing cells usually undergoing multiple dynamic cycles of bleb formation and retraction (Supplementary Movie 8). Furthermore, membrane blebbing occurred exclusively during mitosis. Blebs are extensions of the cell membrane caused by contractions of the actomyosin cortex to release hydrostatic pressure.[44] In cells dividing under tubular confinement, pressure can only be released at the cell tips that face the two openings of the microtubes. Interestingly, we observed that blebbing started to take place at much earlier mitotic stages in confined cells than in free cells (Figure 4A). Based on time-lapse images of HeLa cells, we noticed that membrane blebbing in confined situations started in prometa-/metaphase and continued throughout cell division (Figure 4A, left two images, and Supplementary Movies 8−10). By contrast, in free cells it occurred exclusively during later cell division stages, mainly cytokinesis, and to a much lesser extent (Figure 4A, right two images, and Supplementary Movie 11). To quantify the spatial positions of membrane protrusions over time, we generated kymographs based on phase-contrast time-lapse images. As shown in the top kymograph in Figure 4B, bleb protrusions (white arrowheads) inside 13 μm microtubes reached lengths of up to ∼10 μm in prometa-/metaphase and more than 35 μm in anaphase (measured from the center of the cell). By contrast, we detected no blebs in free cells in prometa-/metaphase.

DOI: 10.1021/acsnano.6b00461
ACS Nano 2016, 10, 5835−5846

Moreover, the farthest membrane protrusions were limited to ~7 μm in length in anaphase of free cells (Figure 4B, bottom kymograph). Notably, conspicuous membrane blebbing was also observed in confined 3D cultured mitotic RPE1 cells,[28] demonstrating that the observed phenomena are conserved between different types of human cells. Blebbing at the cell tips (the parts of the cell pointing toward the open ends of the tubes) suggested that cells frequently were under internal hydrostatic pressure inside the nanomembranes.

We found that the membrane blebbing and bipolar actin filament distributions inside microtubes were largely prevented by treating cells with blebbistatin,[45] an inhibitor of the force-generating mechanoenzyme myosin II (Figures 4C and 5A, and Supplementary Movies 12−14). Membrane blebs have recently been implicated in mitotic functions, being shown, for example, to contribute to the control of spindle positioning[46] and to act as a partly redundant genome safety mechanism by stabilizing the cleavage furrow during cytokinesis.[47] Indeed, we found that in confined cells, inhibition of blebbing and/or associated processes caused misplacement of the cleavage furrow during cytokinesis and often led to unequally sized asymmetric daughter cells (Supplementary Figure 6A and Supplementary Movie 15). Such phenomena were less pronounced in the absence of blebbistatin (Supplementary Figure 6B).

To better understand the role of membrane blebbing in key mitotic features, such as mitotic progression and chromosome segregation, we compared live-cell movies in the presence or absence of blebbistatin. Movies of mitotic cells when blebbistatin was present exhibited strongly enhanced prometa-/metaphase delays (Figure 5B) in spatially confined cells. These delays were particularly pronounced in cells dividing inside microtubes of intermediate sizes. For instance, in 10−12 μm microtubes, the durations of prometa-/metaphase increased almost 2-fold (p-value = 0.00015). Strikingly, blebbistatin also markedly enhanced genomic instability occurring under tubular confinement. Thus, the percentage of chromosome segregation errors, especially in microtubes of intermediate sizes such as those of 10−12 μm diameters, went up from ~17% to ~60% (Figures 5a′ and C). By contrast, blebbistatin had little impact on the duration of prometa-/metaphase or chromosome segregation errors in unconfined control cells. Thus, prometa-/metaphase lasted 43.1 ± 2.7 min[28] in the absence of blebbistatin compared to 48.3 ± 6.1 min in the presence of blebbistatin (p-value = 0.065; Figure 5B), while chromosome segregation errors occurred in ~6% or ~9% of the anaphase cells in the absence or presence of blebbistatin, respectively (Figure 5C and Supplementary Movie 16). Moreover, in spite of the previously identified impairment of centrosome separation by blebbistatin,[48] treatment with blebbistatin posed no significant hindrance on either chromosome rosette formation or spindle bipolarization in the majority of free cells in our experiments (unperturbed chromosome rosettes in 100% of 17 counted cells and morphologically normal bipolar spindles in >95% of 283 cells, respectively; see also Supplementary Figure 7). This discrepancy could reflect differences in cell lines between the two studies (HeLa cells here versus PtK2/B6−8 cells in the previous report)[48] or the 4-fold lower blebbistatin concentrations we used (25 μM versus 100 μM in the previous report).[48] Thus, the lower concentration of blebbistatin in our study may inhibit some (*e.g.*, membrane blebbing) but not all myosin II-mediated processes. Collectively, our data suggest that blebbing and/or associated processes contribute to accurate chromosome segregation, particularly in cells under tubular confinement. Under these conditions, blebbing and/or associated processes act as a compensatory mechanism to limit the deleterious effects of spatial confinement on chromosome segregation and genome stability.

CONCLUSIONS

We have used "rolled-up" nanotechnology to generate transparent biocompatible 3D structures of tailored tubular geometry with varying diameters. These nanomembrane tubes can be integrated into an experimentally convenient pipeline to investigate the growth and proliferation of mammalian cells under spatial constraints at high resolution. The SiO/SiO_2 bilayer nanomembranes are therefore viable substrates for studying the effects of tubular confinement on various cellular processes including but not limited to geometrically demanding processes such as cell division. The "rolled-up technique" that we have employed integrates nanofilm engineering and standard photolithography processes[34] and can be readily scaled-up to produce microtubes as on-chip arrays. The dimensions (lengths and diameters) and wall thicknesses of these architectures can be precisely controlled, and moreover, the inner surfaces can be functionalized with biomolecules, such as fibronectin. The ease of combining our platform with high- and super-resolution microscopy allowed us to reveal and analyze mitotic alterations under narrow tubular confinement, namely: (1) abnormal spindle morphology including increased lengths of prometa-/metaphase spindles; (2) distorted chromosome arrangements in prometaphase that are in stark contrast to the highly ordered chromosome rosettes occurring in unconfined situations; (3) delays in centrosome separation dynamics during spindle formation; (4) bipolar distribution of the actin/cortactin cell cortex; and (5) enhanced mitotic membrane blebbing that occurs at the cell tips facing the open ends of the microtubes.

Numerous biological systems achieve robustness by employing feedback loops.[49,50] Our observations suggest that the mechano- and/or geometry-sensing system of redistributing proteins in response to spatial constraints may be part of such a feedback mechanism that monitors cell shape and/or associated features during mitosis. Indeed, we speculate that cells may sense and respond to spatial strain in the cortex, perhaps by opening ion channels or by stretching cortical cytoskeletal proteins such as actin to create new binding sites[51,52] and triggering the recruitment of contractile/cortical and/or other proteins to further translate the signal. Such scenarios will be interesting to investigate in future studies.

The effects of tubular constraints that we have observed on key mitotic features such as the spindle, chromosome rosettes and centrosome separation, are consistent with the previously reported impact of spatial constraints on mammalian cell division.[14,25] Given that perturbations of spindle morphology and dynamics impair the "search-and-capture" interactions between microtubules and kinetochores,[53,54] our findings could help explain the subsequent prometa-/metaphase delays and the increased chromosomal instability observed previously in such contexts.[28] Indeed, the information presented herein provides valuable clues as to what potential causes could trigger the high percentage of chromosome segregation errors (CSEs) occurring inside microtubes. Intriguingly, our findings suggest that some mitosis-specific responses, especially membrane blebs, are involved in limiting chromosome segregation errors in certain confined environments. Such responses might also

DOI: 10.1021/acsnano.6b00461
ACS Nano 2016, 10, 5835−5846

operate within the context of certain steps during metastasis when large cancer cells undergo tubular confinement inside blood arterioles and capillaries. It will thus be interesting to explore precisely how mitotic processes as diverse as SAC activation, cortex bipolarization, and membrane blebbing are orchestrated to help limit genome instability specifically in cells dividing in 3D environments under such types of spatial confinement. Our 3D nanomembrane technology could provide an excellent platform for such future studies. Notably, evidence has emerged that primary and secondary tumors can vary in their genomic/chromosomal makeup.[8−10] It will be interesting in the future to see whether aberrant mitotic processes, occurring during intravascular proliferation, could in part explain these differences.

In summary, our study provides an in-depth characterization of a versatile rolled-up nanomembrane platform that can be used as a powerful tool for live single-cell studies. Indeed, the system can be applied to virtually every cellular pathway amenable to high- and/or super-resolution microscopy. Rolled-up nanomembranes are highly adaptable in their design and could easily be combined with various other technologies, such as electronic circuits and microfluidic lab-in-a-tube systems.[29] Moreover, we believe that the array setup of the tubular nanomembranes has considerable potential to be exploited for tissue engineering/development and high-throughput drug screening.

METHODS AND EXPERIMENTAL SECTION

Fabricating Microtubes in On-Chip Format for Mammalian Cell Culture. We fabricated microtubes by rolling-up nanomembranes on square glass slides (18 mm in length; thickness, 170 μm). To prepare sacrificial layer patterns, a 2.4 μm thick positive photoresist (AR P-3510, Allresist GmbH) film was first prepared on the glass slides by spin-coating at 3500 rpm for 35 s followed by a baking step at 90 °C for 5 min on a hot plate. A conventional photolithography step using a contact mode mask aligner (MA56, SUSS MicroTec AG) was exploited to produce designed patterns on the glass slides. After that, SiO and SiO_2 nanomembranes were deposited onto the patterns with an electron beam evaporation system (BOC Edwards FL400, Germany) at a glancing angle of 30° and deposition rates of 5.0 Å/s for SiO and 0.5 Å/s for SiO_2, respectively. To achieve microtubes with diameters ranging from 4 to 20 μm, SiO/SiO_2 bilayers of thicknesses between 25 and 100 nm were deposited. The binanomembranes were immediately rolled-up into microtubes by under-etching the sacrificial layers in an acetone solution for a few seconds. The samples were dried by a super critical point dryer to prevent the tubes from collapsing. To strengthen the microtubes, they were further coated with an Al_2O_3 layer of 15 nm in thickness, using atomic layer deposition (Savannah 100, Cambridge NanoTech Inc.) at 80 °C.

Functionalization of the Microtubes with Fibronectin. To grow a monolayer of octadecanylphosphonic acid on the microtube arrays, the samples were incubated in a toluene solution (50 μM) overnight, followed by a thorough rinse with toluene, acetone and water. The samples were then immersed into a 1× PBS solution, containing 100 mM *N*-(3-(dimethylamino)propyl)-*N*′-ethylcarbodiimide hydrochloride (EDC) and 25 mM *N*-hydroxylsulfosuccinimide (NHS) for 1 h followed by an incubation step with 20 μg mL^{-1} fibronectin for 1 h at 37 °C.

Cell Culture and Synchronization. Untagged HeLa cells and HeLa cells, stably transfected with histone H2B-mCherry and GFP-tubulin[55] or centrin1-GFP,[56] were cultured on a T25 (25 cm^2) flask in complete medium (Dulbecco's Modified Eagle Medium (DMEM) (Sigma-Aldrich), 2 mM L-glutamine (Invitrogen), 10% fetal bovine serum (FBS, Sigma-Aldrich), and 1% antibiotics) at 37 °C in a humidified incubator containing 5% CO_2. To maintain the stably transfected cells, 0.4 mg mL^{-1} G418 (GFP-tubulin, centrin1-GFP) or 0.5 μg mL^{-1} puromycin (H2B-mCherry) were used. RPE1 cells were grown in full DMEM medium, supplemented with 2 mM L-glutamine, 10% FBS, and 1% antibiotic mixture (penicillin/streptomycin, Invitrogen). To allow cell migration into the microtubes, cells at a concentration of 2 × 10^5 cells mL^{-3} were plated onto microtube arrays and cultured for 1−2 days. After that, cells growing outside the tubes were removed by a brief trypsinization step. To enrich mitotic cells in the microtubes, a double-thymidine block[57] (2 mM thymidine) was performed to synchronize cells in G1/S phase. After release from the double-thymidine block, the cells were further grown in complete medium for 7−8 h before imaging them with optical microscopy.

Inhibitor Treatments. Blebbistatin (Sigma-Aldrich) was used at a final concentration of 25 μM and was added 1 h before cells entered mitosis.

Fixation and Staining for Optical Microscopy. A fixative solution containing 3% paraformaldehyde, 1% Triton X-100, and 0.25% glutaraldehyde in cytoskeleton buffer (a mixture of 10 mM PIPES pH 6.8, 300 mM sucrose, 2 mM $MgCl_2$, 100 mM NaCl, and 1 mM EGTA) was used to fix cells for 15 min. 1× PBS solution, containing 1 μM phalloidin-FITC (P5282, Sigma-Aldrich) and 1 μM DAPI (4, 6-diamidino-2-phenylindole), was used to stain F-actin and DNA, respectively. Cortactin was immunolabeled using primary rabbit antibodies (1:200; ab11066, Abcam plc.) and secondary goat antirabbit-Alexa594 antibody (1:1000; A-11037, Invitrogen GmbH).

Live-Cell Imaging. For time-lapse imaging, the microtube arrays were mounted on 35 mm dishes (MatTek Corporation). The cells were then plated onto these arrays and treated with/without chemical reagents according to the method mentioned above. Imaging was performed in a heated and humidified chamber (stabilized at 37 °C and containing 5% CO_2). Cells were imaged, using an Axio Observer Z1 inverted microscope (Zeiss, 40× objective). For time-lapse imaging of cell division events, we captured one frame every 5−15 min, depending on the specific experiment. Z-stacks (0.5−1.0 μm) of the mitotic apparatus (entire volume) were obtained every 5 min with a PLANAPO 40× objective. The images were deconvolved using Huygens and analyzed using Fiji.[58] Images represent maximum-intensity projections of all *z*-planes.

High- and Super-Resolution Imaging. Entrapped and free HeLa cells were fixed in prometaphase and, in the case of untagged HeLa cells, stained with DAPI and phalloidin−FITC. Confocal imaging was performed with an LSM 700 inverted microscope (Zeiss) equipped with a Zeiss C-Apochromat 60 × 1.2 W objective, using 405, 488, and 594 nm laser lines for excitation, a 1532 × 1532 pixel frame size at a rate of 0.42 μs per pixel and a 1 Airy Unit pinhole diameter. Z-sections taken every 410 nm covering the entire cell were projected (maximum intensity).

Super-resolution 3D SIM imaging of phalloidin-FITC (F-actin) and DAPI as well as H2B-mCherry and GFP-tubulin was acquired using a Deltavision OMX 3D SIM System V3 from Applied Precision (a GE Healthcare company) equipped with 3 EMCCD Cascade cameras from Photometrics, 405, 488, 592.5 nm diode laser illumination, an Olympus PlanSApo 100× 1.40 NA oil objective, and standard excitation and emission filter sets. Imaging of each channel was performed sequentially using three angles and five phase shifts of the illumination pattern as described in Gustafsson et al., 2008.[59] The refractive index of the immersion oil (Cargille) was adjusted to 1.514 to minimize spherical aberrations. Sections were acquired at 0.125 μm *z* steps.

Raw OMX data were reconstructed and channel registered in the SoftWoRx software (Applied Precision, a GE Healthcare company). Reconstructions were carried out using channel-specific Optical Transfer Functions (OTFs) and channel-specific K0 angles. OTFs were generated within the SoftWoRx software by imaging 100 nm beads (Life Technologies) using appropriate immersion oils to match the data. Channel registration was carried out using the Image Registration parameters generated within the SoftWoRx software and checked for accuracy by imaging Tetraspeck beads (Life Technologies). Channel registration was accurate to within one pixel. Further data analysis was performed using Fiji.[58]

DOI: 10.1021/acsnano.6b00461
ACS Nano 2016, 10, 5835−5846

3D Reconstruction of Chromosomes. *Z*-stack images were deconvolved with Huygens Professional 4.1 (SVI), and 3D reconstruction was performed by its module surface renderer.

Statistics and Computational Analysis. Means ± standard deviations presented herein were obtained by comparing at least three independently performed experiments. Student's *t*-tests, as indicated in the figure legends, were performed to evaluate statistical differences between two groups, as indicated in the Figures. P-values ≥ 0.05 were considered nonsignificant.

The 3D Euclidean distances between centrosomes were calculated using Ace 3D, a visualization and analysis plugin for Fiji[58] that uses 3D Object Counter[60] to create multidimensional centroid maps for analysis (available on request).

The 3D temporal evolution of spindle lengths (mean distances between centrosomes ± SD) was plotted against time using OriginPro 9.0.0. The linear portion of the curves was selected by Data Selector tool and fit by linear regressions utilizing the OriginPro 9.0.0 programming environment with a least-squares fitting algorithm.

ASSOCIATED CONTENT

Supporting Information

The Supporting Information is available free of charge on the ACS Publications website at DOI: 10.1021/acsnano.6b00461.

Movie 1: 3D-rotation of a reconstructed prometaphase chromosome rosette in unconfined conditions (AVI)

Movie 2: 3D-rotation of a reconstructed prometaphase chromosome rosette inside a 9 μm microtube (AVI)

Movie 3: 3D-rotation of a reconstructed prometaphase chromosome rosette inside a 13 μm microtube (AVI)

Movie 4: 3D-rotation of a reconstructed prometaphase chromosome rosette inside a 17 μm microtube (AVI)

Movie 5: Time-lapse movie of a centrin1-GFP (green) expressing HeLa cell undergoing mitosis without confinement (AVI)

Movie 6: Time-lapse movie of a centrin1-GFP (green) expressing HeLa cell undergoing mitosis inside a 9 μm microtube (selected frames shown in Figure 2A) (AVI)

Movie 7: 3D-rotation view of mitotic HeLa cells expressing H2B-mCherry (red) and immunolabelled for cortactin (green) in unconfined conditions (left) and inside a 9 μm microtube (right) (AVI)

Movie 8: Phase-contrast and fluorescent time-lapse video of a H2BmCherry (red) and GFP-tubulin (green) expressing HeLa cell dividing inside a 9 μm microtube (AVI)

Movie 9: 3D-SIM rotation of the image shown in Figure 4c' left (AVI)

Movie 10: 3D-SIM rotation of the image shown in Figure 4c' right (AVI)

Movie 11: Phase-contrast and fluorescent time-lapse video of a H2BmCherry (red) and GFP-tubulin (green) expressing HeLa cell dividing in unconfined conditions (AVI)

Movie 12: 3D-SIM rotation of the image shown in Figure 4c" left (AVI)

Movie 13: 3D-SIM rotation of the image shown in Figure 4c" right (AVI)

Movie 14: Phase-contrast and fluorescent time-lapse video of a H2B-mCherry (red) expressing HeLa cell dividing inside a 16 μm microtube in the presence of 25 μM blebbistatin (selected frames are presented in Figure 5A) (AVI)

Movie 15: Phase-contrast and fluorescent time-lapse video of a H2B-mCherry (red) expressing HeLa cell dividing inside a 17 μm microtube in the presence of 25 μM blebbistatin (AVI)

Movie 16: Phase-contrast and fluorescent time-lapse video of a H2B-mCherry (red) expressing HeLa cell dividing in unconfined conditions in the presence of 25 μM blebbistatin (AVI)

A 3D schematic representation of 1D confinement using planar surfaces applied to 2D-cultured cells. Super-resolution fluorescent images and 3D reconstruction of chromosome rosettes together with microtubules in free and confined HeLa cells. Explanatory image illustrating the features of a Fiji plugin developed for automated 3D centrosome mapping and plots of the quantification of 3D temporal evolution of spindle lengths as indicated by positions of centrosome. Fluorescent (time-lapse) images showing the bipolarized distribution of actin cortex in an RPE1 cell under confinement and spindle rotation, centrin1-GFP-expressing HeLa cells showing increased intercentrosome distances, and mis-/proper-placement of cleavage furrow during cytokinesis in HeLa cells with/without blebbistatin. Confocal images showing the chromosome rosettes formed in blebbistatin-treated free HeLa cells (PDF)

AUTHOR INFORMATION

Corresponding Authors

*E-mail: wang.xi227@gmail.com.

*E-mail: cs681@cam.ac.uk and christine.schmidt@manchester.ac.uk.

Present Addresses

[○]Centre for Advanced 2D Materials and Graphene Research Centre, National University of Singapore, Blk S14, Level 1 Science Drive 2, Singapore 117542.

[▽]Max Planck Institute for Intelligent Systems, Heisenbergstr. 3, 70569 Stuttgart, Germany; Institució Catalana de Recerca i Estudis Avancats (ICREA), Pg. Lluís Companys 23, 08010 Barcelona, Spain; Institut de Bioenginyeria de Catalunya (IBEC), Baldiri i Reixac 10-12, 08028 Barcelona, Spain.

[ψ]Manchester Cancer Research Centre, University of Manchester, Wilmslow Road, M20 4QL, United Kingdom.

Notes

The authors declare no competing financial interest.

ACKNOWLEDGMENTS

We thank the Gurdon Institute Imaging Facility for microscopy support; Daniel Gerlich for the GFP-tubulin/H2B-mCherry expressing HeLa cells and Helder Maiato for the HeLa centrin1-GFP cell line; Jon Pines, Takahiro Matsusaka, and Paola Marco for comments; Marlitt Viehrig, Anka Kempe, and Britta Koch for support in cell culture, image analysis, and microcavities preparation; Chenglin Yan and Elliot Smith for support in the experiments; Ronny Engelhard for technical support; and Daniel Grimm for support in the clean room facilities. We thank Ralph Träger for providing 3D schematic diagrams and Xumei Gao for helping to make the schematic illustration in Figure 1A. The research leading to these results has received funding from the European Research Council under the European Union's Seventh Framework Programme (FP7/2007-2013)/ERC grant agreement no. 311529 (S.S.) and the Volkswagen Foundation no. 86 362 (S.S. and W.X.), a FEBS Return-to-Europe fellowship (C.K.S.), the Wellcome Trust (092096/Z/10/Z for N.L.; 094587/Z/10/Z for R.B.),

DOI: 10.1021/acsnano.6b00461
ACS Nano 2016, 10, 5835−5846

and a European Research Council (ERC) Starting Researcher Grant (R.E.C.-S.; SYSGRO). O.G.S. acknowledges financial support from the DFG Research Unit 1713 "Sensorische Mikro und Nanosysteme". D.H.G. acknowledges funding from the Alexander von Humboldt Foundation and the U.S. National Science Foundation (Grants: CMMI 1200241 and CBET-1442014). Research in the S.P.J. laboratory is funded by Cancer Research U.K., the ERC, and the European Community Seventh Framework Programme (DDResponse), with core infrastructure provided by Cancer Research U.K. and the Wellcome Trust.

REFERENCES

(1) Weigelin, B.; Bakker, G.-J.; Friedl, P. Intravital Third Harmonic Generation Microscopy of Collective Melanoma Cell Invasion. *IntraVital* **2012**, *1*, 32−43.
(2) Wong, C. W.; Song, C.; Grimes, M. M.; Fu, W.; Dewhirst, M. W.; Muschel, R. J.; Al-Mehdi, A.-B. Intravascular Location of Breast Cancer Cells after Spontaneous Metastasis to the Lung. *Am. J. Pathol.* **2002**, *161*, 749−753.
(3) Al-Mehdi, A. B.; Tozawa, K.; Fisher, A. B.; Shientag, L.; Lee, A.; Muschel, R. J. Intravascular Origin of Metastasis from the Proliferation of Endothelium-Attached Tumor Cells: A New Model for Metastasis. *Nat. Med.* **2000**, *6*, 100−102.
(4) Miles, F. L.; Pruitt, F. L.; van Golen, K. L.; Cooper, C. R. Stepping out of the Flow: Capillary Extravasation in Cancer Metastasis. *Clin. Exp. Metastasis* **2008**, *25*, 305−324.
(5) Chambers, A. F.; Groom, A. C.; MacDonald, I. C. Metastasis: Dissemination and Growth of Cancer Cells in Metastatic Sites. *Nat. Rev. Cancer* **2002**, *2*, 563−572.
(6) Suetsugu, A.; Jiang, P.; Moriwaki, H.; Saji, S.; Bouvet, M.; Hoffman, R. M. Imaging Nuclear - Cytoplasm Dynamics of Cancer Cells in the Intravascular Niche of Live Mice. *Anticancer Res.* **2013**, *33*, 4229−4236.
(7) Zhang, Q.; Yang, M.; Shen, J.; Gerhold, L. M.; Hoffman, R. M.; Xing, H. R. The Role of the Intravascular Microenvironment in Spontaneous Metastasis Development. *Int. J. Cancer* **2010**, *126*, 2534−2541.
(8) Nguyen, D. X.; Massague, J. Genetic Determinants of Cancer Metastasis. *Nat. Rev. Genet.* **2007**, *8*, 341−352.
(9) Crissman, J. D.; Hatfield, J. S.; Menter, D. G.; Sloane, B.; Honn, K. V. Morphological Study of the Interaction of Intravascular Tumor Cells with Endothelial Cells and Subendothelial Matrix. *Cancer Res.* **1988**, *48*, 4065−4072.
(10) Dao, V. T.; Dupuy, A. G.; Gavet, O.; Caron, E.; de Gunzburg, J. Dynamic Changes in Rap1 Activity Are Required for Cell Retraction and Spreading during Mitosis. *J. Cell Sci.* **2009**, *122*, 2996−3004.
(11) Kunda, P.; Baum, B. The Actin Cytoskeleton in Spindle Assembly and Positioning. *Trends Cell Biol.* **2009**, *19*, 174−179.
(12) Matthews, H. K.; Baum, B. The Metastatic Cancer Cell Cortex: An Adaptation to Enhance Robust Cell Division in Novel Environments? *BioEssays* **2012**, *34*, 1017−1020.
(13) Clark, A. G.; Dierkes, K.; Paluch, E. K. Monitoring Actin Cortex Thickness in Live Cells. *Biophys. J.* **2013**, *105*, 570−580.
(14) Lancaster, O. M.; Le Berre, M.; Dimitracopoulos, A.; Bonazzi, D.; Zlotek-Zlotkiewicz, E.; Picone, R.; Duke, T.; Piel, M.; Baum, B. Mitotic Rounding Alters Cell Geometry to Ensure Efficient Bipolar Spindle Formation. *Dev. Cell* **2013**, *25*, 270−283.
(15) Théry, M.; Bornens, M. Get Round and Stiff for Mitosis. *HFSP J.* **2008**, *2*, 65−71.
(16) Fededa, J. P.; Gerlich, D. W. Molecular Control of Animal Cell Cytokinesis. *Nat. Cell Biol.* **2012**, *14*, 440−447.
(17) Magidson, V.; O'Connell, C. B.; Loncarek, J.; Paul, R.; Mogilner, A.; Khodjakov, A. The Spatial Arrangement of Chromosomes during Prometaphase Facilitates Spindle Assembly. *Cell* **2011**, *146*, 555−567.
(18) Tanenbaum, M. E.; Medema, R. H. Mechanisms of Centrosome Separation and Bipolar Spindle Assembly. *Dev. Cell* **2010**, *19*, 797−806.
(19) Lancaster, O. M.; Baum, B. Shaping up to Divide: Coordinating Actin and Microtubule Cytoskeletal Remodelling during Mitosis. *Semin. Cell Dev. Biol.* **2014**, *34*, 109−115.
(20) Jallepalli, P. V.; Lengauer, C. Chromosome Segregation and Cancer: Cutting through the Mystery. *Nat. Rev. Cancer* **2001**, *1*, 109−117.
(21) Santaguida, S.; Amon, A. Short- and Long-Term Effects of Chromosome Mis-Segregation and Aneuploidy. *Nat. Rev. Mol. Cell Biol.* **2015**, *16*, 473−485.
(22) Thery, M.; Racine, V.; Pepin, A.; Piel, M.; Chen, Y.; Sibarita, J. B.; Bornens, M. The Extracellular Matrix Guides the Orientation of the Cell Division Axis. *Nat. Cell Biol.* **2005**, *7*, 947−953.
(23) Fink, J.; Carpi, N.; Betz, T.; Betard, A.; Chebah, M.; Azioune, A.; Bornens, M.; Sykes, C.; Fetler, L.; Cuvelier, D.; Piel, M. External Forces Control Mitotic Spindle Positioning. *Nat. Cell Biol.* **2011**, *13*, 771−778.
(24) Thery, M.; Jimenez-Dalmaroni, A.; Racine, V.; Bornens, M.; Julicher, F. Experimental and Theoretical Study of Mitotic Spindle Orientation. *Nature* **2007**, *447*, 493−496.
(25) Tse, H. T. K.; Weaver, W. M.; Di Carlo, D. Increased Asymmetric and Multi-Daughter Cell Division in Mechanically Confined Microenvironments. *PLoS One* **2012**, *7*, e38986.
(26) Dumont, S.; Mitchison, T. J. Compression Regulates Mitotic Spindle Length by a Mechanochemical Switch at the Poles. *Curr. Biol.* **2009**, *19*, 1086−1095.
(27) Kwag, H. R.; Serbo, J. V.; Korangath, P.; Sukumar, S.; Romer, L. H.; Gracias, D. H. A Self-Folding Hydrogel *In Vitro* Model for Ductal Carcinoma. *Tissue Eng., Part C* **2016**, *22*, 398−407.
(28) Xi, W.; Schmidt, C. K.; Sanchez, S.; Gracias, D. H.; Carazo-Salas, R. E.; Jackson, S. P.; Schmidt, O. G. Rolled-Up Functionalized Nanomembranes as Three-Dimensional Cavities for Single Cell Studies. *Nano Lett.* **2014**, *14*, 4197−4204.
(29) Smith, E. J.; Xi, W.; Makarov, D.; Monch, I.; Harazim, S.; Quinones, V. A. B.; Schmidt, C. K.; Mei, Y. F.; Sanchez, S.; Schmidt, O. G. Lab-in-a-Tube: Ultracompact Components for On-Chip Capture and Detection of Individual Micro-/Nanoorganisms. *Lab Chip* **2012**, *12*, 1917−1931.
(30) Harazim, S. M.; Xi, W.; Schmidt, C. K.; Sanchez, S.; Schmidt, O. G. Fabrication and Applications of Large Arrays of Multifunctional Rolled-Up SiO/SiO_2 Microtubes. *J. Mater. Chem.* **2012**, *22*, 2878−2884.
(31) Regehr, K. J.; Domenech, M.; Koepsel, J. T.; Carver, K. C.; Ellison-Zelski, S. J.; Murphy, W. L.; Schuler, L. A.; Alarid, E. T.; Beebe, D. J. Biological Implications of Polydimethylsiloxane-Based Microfluidic Cell Culture. *Lab Chip* **2009**, *9*, 2132−2139.
(32) Fredrickson, C. K.; Fan, Z. H. Macro-to-Micro Interfaces for Microfluidic Devices. *Lab Chip* **2004**, *4*, 526−533.
(33) Halldorsson, S.; Lucumi, E.; Gómez-Sjöberg, R.; Fleming, R. M. T. Advantages and Challenges of Microfluidic Cell Culture in Polydimethylsiloxane Devices. *Biosens. Bioelectron.* **2015**, *63*, 218−231.
(34) Mei, Y. F.; Huang, G. S.; Solovev, A. A.; Urena, E. B.; Moench, I.; Ding, F.; Reindl, T.; Fu, R. K. Y.; Chu, P. K.; Schmidt, O. G. Versatile Approach for Integrative and Functionalized Tubes by Strain Engineering of Nanomembranes on Polymers. *Adv. Mater.* **2008**, *20*, 4085−4090.
(35) Huang, G. S.; Mei, Y. F.; Thurmer, D. J.; Coric, E.; Schmidt, O. G. Rolled-Up Transparent Microtubes as Two-Dimensionally Confined Culture Scaffolds of Individual Yeast Cells. *Lab Chip* **2009**, *9*, 263−268.
(36) Schulze, S.; Huang, G. S.; Krause, M.; Aubyn, D.; Quinones, V. A. B.; Schmidt, C. K.; Mei, Y. F.; Schmidt, O. G. Morphological Differentiation of Neurons on Microtopographic Substrates Fabricated by Rolled-Up Nanotechnology. *Adv. Eng. Mater.* **2010**, *12*, B558−B564.
(37) Yamauchi, K.; Yang, M.; Jiang, P.; Yamamoto, N.; Xu, M.; Amoh, Y.; Tsuji, K.; Bouvet, M.; Tsuchiya, H.; Tomita, K.; Moossa, A. R.; Hoffman, R. M. Real-Time *In Vivo* Dual-Color Imaging of Intracapillary Cancer Cell and Nucleus Deformation and Migration. *Cancer Res.* **2005**, *65*, 4246−4252.

DOI: 10.1021/acsnano.6b00461
ACS Nano 2016, 10, 5835−5846

(38) Carreno, S.; Kouranti, I.; Glusman, E. S.; Fuller, M. T.; Echard, A.; Payre, F. Moesin and Its Activating Kinase Slik Are Required for Cortical Stability and Microtubule Organization in Mitotic Cells. *J. Cell Biol.* **2008**, *180*, 739−746.
(39) Kunda, P.; Pelling, A. E.; Liu, T.; Baum, B. Moesin Controls Cortical Rigidity, Cell Rounding, and Spindle Morphogenesis during Mitosis. *Curr. Biol.* **2008**, *18*, 91−101.
(40) Thery, M.; Bornens, M. Cell Shape and Cell Division. *Curr. Opin. Cell Biol.* **2006**, *18*, 648−657.
(41) Baumann, K. The Division Belt. *Nat. Rev. Mol. Cell Biol.* **2011**, *12*, 622−622.
(42) Musacchio, A.; Salmon, E. D. The Spindle-Assembly Checkpoint in Space and Time. *Nat. Rev. Mol. Cell Biol.* **2007**, *8*, 379−393.
(43) Wang, N.; Butler, J.; Ingber, D. Mechanotransduction Across the Cell Surface and through the Cytoskeleton. *Science* **1993**, *260*, 1124−1127.
(44) Charras, G.; Paluch, E. Blebs Lead the Way: How to Migrate without Lamellipodia. *Nat. Rev. Mol. Cell Biol.* **2008**, *9*, 730−736.
(45) Straight, A. F.; Cheung, A.; Limouze, J.; Chen, I.; Westwood, N. J.; Sellers, J. R.; Mitchison, T. J. Dissecting Temporal and Spatial Control of Cytokinesis with a Myosin II Inhibitor. *Science* **2003**, *299*, 1743−1747.
(46) Kiyomitsu, T.; Cheeseman, I. M. Cortical Dynein and Asymmetric Membrane Elongation Coordinately Position the Spindle in Anaphase. *Cell* **2013**, *154*, 391−402.
(47) Sedzinski, J.; Biro, M.; Oswald, A.; Tinevez, J. Y.; Salbreux, G.; Paluch, E. Polar Actomyosin Contractility Destabilizes the Position of the Cytokinetic Furrow. *Nature* **2011**, *476*, 462−466.
(48) Rosenblatt, J.; Cramer, L. P.; Baum, B.; McGee, K. M. Myosin II-Dependent Cortical Movement Is Required for Centrosome Separation and Positioning during Mitotic Spindle Assembly. *Cell* **2004**, *117*, 361−372.
(49) Brandman, O.; Ferrell, J. E.; Li, R.; Meyer, T. Interlinked Fast and Slow Positive Feedback Loops Drive Reliable Cell Decisions. *Science* **2005**, *310*, 496−498.
(50) Stelling, J.; Sauer, U.; Szallasi, Z.; Doyle Iii, F. J.; Doyle, J. Robustness of Cellular Functions. *Cell* **2004**, *118*, 675−685.
(51) Janmey, P. A.; Weitz, D. A. Dealing with Mechanics: Mechanisms of Force Transduction in Cells. *Trends Biochem. Sci.* **2004**, *29*, 364−370.
(52) Orr, A. W.; Helmke, B. P.; Blackman, B. R.; Schwartz, M. A. Mechanisms of Mechanotransduction. *Dev. Cell* **2006**, *10*, 11−20.
(53) Paul, R.; Wollman, R.; Silkworth, W. T.; Nardi, I. K.; Cimini, D.; Mogilner, A. Computer Simulations Predict That Chromosome Movements and Rotations Accelerate Mitotic Spindle Assembly without Compromising Accuracy. *Proc. Natl. Acad. Sci. U. S. A.* **2009**, *106*, 15708−15713.
(54) Wollman, R.; Cytrynbaum, E. N.; Jones, J. T.; Meyer, T.; Scholey, J. M.; Mogilner, A. Efficient Chromosome Capture Requires a Bias in the 'Search-and-Capture' Process during Mitotic-Spindle Assembly. *Curr. Biol.* **2005**, *15*, 828−832.
(55) Steigemann, P.; Wurzenberger, C.; Schmitz, M. H. A.; Held, M.; Guizetti, J.; Maar, S.; Gerlich, D. W. Aurora B-Mediated Abscission Checkpoint Protects against Tetraploidization. *Cell* **2009**, *136*, 473−484.
(56) Logarinho, E.; Maffini, S.; Barisic, M.; Marques, A.; Toso, A.; Meraldi, P.; Maiato, H. CLASPs Prevent Irreversible Multipolarity by Ensuring Spindle-Pole Resistance to Traction Forces during Chromosome Alignment. *Nat. Cell Biol.* **2012**, *14*, 295−303.
(57) Santaguida, S.; Tighe, A.; D'Alise, A. M.; Taylor, S. S.; Musacchio, A. Dissecting the Role of MPS1 in Chromosome Biorientation and the Spindle Checkpoint through the Small Molecule Inhibitor Reversine. *J. Cell Biol.* **2010**, *190*, 73−87.
(58) Schindelin, J.; Arganda-Carreras, I.; Frise, E.; Kaynig, V.; Longair, M.; Pietzsch, T.; Preibisch, S.; Rueden, C.; Saalfeld, S.; Schmid, B.; Tinevez, J.-Y.; White, D. J.; Hartenstein, V.; Eliceiri, K.; Tomancak, P.; Cardona, A. Fiji: An Open-Source Platform for Biological-Image Analysis. *Nat. Methods* **2012**, *9*, 676−682.
(59) Gustafsson, M. G. L.; Shao, L.; Carlton, P. M.; Wang, C. J. R.; Golubovskaya, I. N.; Cande, W. Z.; Agard, D. A.; Sedat, J. W. Three-Dimensional Resolution Doubling in Wide-Field Fluorescence Microscopy by Structured Illumination. *Biophys. J.* **2008**, *94*, 4957−4970.
(60) Bolte, S.; Cordelières, F. P. A Guided Tour into Subcellular Colocalization Analysis in Light Microscopy. *J. Microsc.* **2006**, *224*, 213−232.

DOI: 10.1021/acsnano.6b00461
ACS Nano 2016, 10, 5835−5846